NASA/TM-20240003948

Analytical Simulation of Effects of Local Mechanisms and Microstructure on Creep Response of Unidirectional Ceramic Matrix Composites

Robert K. Goldberg, Amjad S. Almansour, and Roy M. Sullivan
Glenn Research Center, Cleveland, Ohio

June 2024

NASA STI Program Report Series

Since its founding, NASA has been dedicated to the advancement of aeronautics and space science. The NASA scientific and technical information (STI) program plays a key part in helping NASA maintain this important role.

The NASA STI program operates under the auspices of the Agency Chief Information Officer. It collects, organizes, provides for archiving, and disseminates NASA's STI. The NASA STI program provides access to the NTRS Registered and its public interface, the NASA Technical Reports Server, thus providing one of the largest collections of aeronautical and space science STI in the world. Results are published in both non-NASA channels and by NASA in the NASA STI Report Series, which includes the following report types:

- TECHNICAL PUBLICATION.
  Reports of completed research or a major significant phase of research that present the results of NASA Programs and include extensive data or theoretical analysis. Includes compilations of significant scientific and technical data and information deemed to be of continuing reference value. NASA counterpart of peer-reviewed formal professional papers but has less stringent limitations on manuscript length and extent of graphic presentations.

- TECHNICAL MEMORANDUM.
  Scientific and technical findings that are preliminary or of specialized interest, e.g., quick release reports, working papers, and bibliographies that contain minimal annotation. Does not contain extensive analysis.

- CONTRACTOR REPORT.
  Scientific and technical findings by NASA-sponsored contractors and grantees.

- CONTRACTOR REPORT.
  Scientific and technical findings by NASA-sponsored contractors and grantees.

- CONFERENCE PUBLICATION.
  Collected papers from scientific and technical conferences, symposia, seminars, or other meetings sponsored or co-sponsored by NASA.

- SPECIAL PUBLICATION.
  Scientific, technical, or historical information from NASA programs, projects, and missions, often concerned with subjects having substantial public interest.

- TECHNICAL TRANSLATION.
  English-language translations of foreign scientific and technical material pertinent to NASA's mission.

Specialized services also include organizing and publishing research results, distributing specialized research announcements and feeds, providing information desk and personal search support, and enabling data exchange services.

For more information about the NASA STI program, see the following:

- Access the NASA STI program home page at http://www.sti.nasa.gov

NASA/TM-20240003948

Analytical Simulation of Effects of Local Mechanisms and Microstructure on Creep Response of Unidirectional Ceramic Matrix Composites

Robert K. Goldberg, Amjad S. Almansour, and Roy M. Sullivan
Glenn Research Center, Cleveland, Ohio

National Aeronautics and
Space Administration

Glenn Research Center
Cleveland, Ohio 44135

June 2024

Acknowledgments

This work was funded by the Transformational Tools and Technologies Project under NASA's Aeronautics Research Mission Directorate.

This report contains preliminary findings, subject to revision as analysis proceeds.

Level of Review: This material has been technically reviewed by technical management.

This report is available in electronic form at https://www.sti.nasa.gov/ and https://ntrs.nasa.gov/

NASA STI Program/Mail Stop 050
NASA Langley Research Center
Hampton, VA 23681-2199

Analytical Simulation of Effects of Local Mechanisms and Microstructure on Creep Response of Unidirectional Ceramic Matrix Composites

Robert K. Goldberg, Amjad S. Almansour, and Roy M. Sullivan
National Aeronautics and Space Administration
Glenn Research Center
Cleveland, Ohio 44135

Summary

A micromechanics-based method has been developed to analyze the creep response of uncoated ceramic matrix minicomposites. Although the global stress level at which the creep response is analyzed is lower than the composite proportional limit, local stresses are assumed to be high enough that localized damage is present in the composite in the form of matrix microcracks. To model the composite creep response, including the effects of matrix cracking, a fiber shear lag-based methodology is employed. In this approach, stresses are assumed to vary in the fiber as a function of time and distance from the crack plane. The varying stresses are then used to compute the overall creep strain for the composite. Various assumptions regarding the level of matrix microcracking in the composite and the level of creep in the fiber and matrix in various portions of the composite unit cell are also examined. The creep response of the fiber is modeled using a linear Burgers model. The model is applied to a SiC_f/SiC unidirectional minicomposite system. The computed creep results are compared to experimentally obtained values. The effects of the local fiber volume fraction on the overall creep response of the composite are also studied. This work will allow increased understanding of the key material damage mechanisms and load sharing that take place during creep conditions and can be expanded to provide improved analysis methods for full macrocomposites.

Introduction

The next generation of aircraft gas turbine engines require the capability to maintain structural integrity at very high temperatures. In addition, fuel efficiency considerations require the engine components to be lightweight while still maintaining desired mechanical and thermomechanical properties in the components subject to these elevated temperatures. SiC-based ceramic matrix composites (CMCs) are gaining wider usage as a viable material class for these applications. In order to fully utilize the capabilities of these materials, there is a need to gain a greater understanding of the local damage mechanisms and how they contribute to key features of the material response. As part of this process, material models must be developed that account for these local mechanisms and can simulate the response of ceramic matrix composites under relevant loading conditions.

In previous work by the authors (Ref. 1), a micromechanics-based method based on a fiber shear lag analysis was developed to analyze the fast fracture response of uncoated ceramic matrix minicomposites under room temperature conditions. In the work described in Reference 1, microstructural features such as the ratio of the fiber slip length to the crack spacing were found to be a key parameter driving the stress level at which the proportional limit takes place and the response of the composite after the proportional limit was reached. In addition, irregularities in the composite microstructure and in the geometry and propagation of matrix microcracks were found to have a significant influence on the composite response.

Another important finding of this report, as well as work presented in Reference 2, is that matrix microcracks were present, and affected the composite response, at stresses lower than the proportional limit.

Creep tests on woven SiC/SiC composites with full CVI SiC matrix conducted by Bhatt and Kiser (Ref. 3) at stresses lower than the nominal proportional limit displayed significant variability in the creep response. Potential causes of the variability were hypothesized to be related to local porosities or fiber clustering, which could result in localized stress concentrations. These localized stress concentrations could result in localized matrix cracking. Based on the results of tests such as those described by Bhatt and Kiser (Ref. 3), the development of mechanistic approaches to simulate the creep of composites, including the effects of local damage mechanisms, could help to explain this variability. Ceramic matrix composites require weak fiber coatings between the fiber and the matrix. The weak fiber coatings deflect matrix cracks from propagating through the fibers, which allows intact fibers to bridge matrix cracks and provide damage tolerance and facilitate load transfer from failed fibers to their unbroken nearest neighbors as well as from the cracked matrix to the fibers. They are used to enhance the toughness of a composite that is made from brittle fibers and a brittle matrix (Ref. 4). For composites with localized matrix cracking, the weak fiber coatings can significantly affect the composite response.

One difficulty in studying CMCs is that procuring test specimens of full-sized macrocomposites can be very time consuming and costly. As an accelerated and simple testing alternative, studying minicomposites, effectively a fiber tow coated with a weak coating and a matrix, can provide a convenient method to examine the key response features of CMCs in a rapid, cost-efficient manner.

There have been several analytical studies to model the creep response of ceramic matrix composites and minicomposites. In Almansour and Morscher (Ref. 5), a number of minicomposites with CVD-SiC matrices, Hi-Nicalon™ and Hi-Nicalon-S™ fibers, and boron nitride fiber coatings were tested under creep conditions at a temperature of 1,200 °C. Both pristine and precracked composites with a variety of fiber volume ratios were tested in air. A creep model was utilized (originally developed by Sauder (Ref. 6)) in which an exponential law was used to model the primary creep and a power law was used to model the secondary creep. Creep tests were conducted on the fiber and matrix and the constants in the creep model were determined from these tests. Both constituents were assumed to creep during the composite creep process. A load sharing model was developed to capture the transfer of load from the matrix to the fiber as both constituents creep. A strain hardening model was developed to account for the changes in stress in each constituent as the creep process progressed. For the pristine minicomposites, no localized matrix cracking was assumed to be present in the material. The effects of fiber type, volume fraction, creep stress and cracking status on the creep response were determined. The creep model was used to track the stress evolution in each of the constituents during creep.

Rugg, et al. (Ref. 7) developed a micromechanics-based model to analyze the creep response of composites both with and without matrix cracks. For the uncracked matrix, a power law formulation was used to model the fiber and matrix creep response. Both the fiber and matrix were assumed to creep, and a load sharing relation was developed to simulate the transfer of load from the matrix to the fiber during the creep process. For minicomposites with cracks, in the areas near the cracks where interfacial load transfer took place between the fiber and the matrix (referred to as the “slip length”), a shear lag-based process was utilized to model the behavior of the composite. Within the slip length region, the fiber stresses decreased in a linear fashion from the plane of the crack until the end of the slip length (where the stress reached a constant homogeneous, continuum level). The slip length was assumed to remain constant during the creep process. Due to the fact that the stress state in the homogeneous stress region was assumed to vary as creep progressed due to load transfer between the fiber and matrix, the effective interfacial shear stress was assumed to vary in order to maintain stress continuity. The varying stress

along the slip length was incorporated into the fiber creep equations to determine the creep strain of the composite along the slip length.

Other types of micromechanical approaches that do not utilize the shear lag and load sharing approaches have been employed to analyze the creep response of ceramic matrix composites. For example, in Mital, et al. (Ref. 8), an approach was developed to model the nonlinear response of ceramic matrix composites through the use of the Generalized Method of Cells. For the creep portion of the model, a Bailey-Norton creep law was generalized to three dimensions and utilized to model the creep response of both the fiber and the matrix. In the Generalized Method of Cells, a unit cell of the composite is identified, and the unit cell is divided into a series of subcells. Continuity conditions between the various subcells and between periodic unit cells are employed to account for the load transfer between the various constituents. Matrix cracking was not explicitly accounted for within the material model.

Building on this type of approach, in Khafagy, et al. (Ref. 9) a viscoplasticity-based model was used to model the creep of the fiber and matrix constituents. A plastic potential function, and its derivatives with respect to stress, were employed to compute the components of creep strain for both the fiber and matrix. The effective creep strain was computed using a variation of the Norton-Bailey creep law. Matrix damage was accounted for by using a continuum damage mechanics model to model the matrix constituent. Note that approaches such as shear lag models to simulate the load transfer between the cracked matrix and the fibers were not utilized in this work. The Generalized Method of Cells was used to compute the overall response of the composite.

Santhosh and Ahmad (Ref. 10) developed a micromechanics approach to simulate the response of ceramic matrix composites under both tensile and creep loading. In this approach, while localized damage in the matrix was accounted for, in the regions near matrix cracks no load transfer was assumed to take place between the fiber and matrix, as opposed to the shear lag type of approach where a certain level of load transfer due to interfacial shear stresses was specified. Specifically, in this model the matrix was assumed to be linear elastic, and the fiber was assumed to have a combination of elastic and inelastic/time-dependent responses. For a composite without damage, a combination of uniform stress and uniform strain assumptions (with appropriate load transfer) were applied to compute the overall response of the composite. For a composite with damage, the approach was extended such that in the damaged region the fiber stress was assumed to be equal to the stress at the crack plane. Empirical equations were developed to compute the length of the damaged region and the evolution of the crack density. This concept is also different from the shear lag approach in which the slip length (the region where interfacial load transfer takes place) is defined based on fiber and matrix constitutive properties. In Santhosh, et al. (Ref. 11), this approach was extended to also permit inelastic, time-dependent deformation of the matrix constituent.

In the current report, the goal of the study is to conduct analytical simulations of the creep response of minicomposites, incorporating effects of localized matrix cracking through the use of a shear lag-based analysis in the damaged region of the composite. The studies presented in this report will concentrate on minicomposites with a fiber volume ratio of approximately 20 percent. However, the effects of varying the fiber volume ratio will be examined. The initial studies described in this report will focus on uncoated composites and also neglect oxidation and other environmental effects.

The report will explore in detail how matrix damage can affect the creep response of the composite, even when the composite is loaded at stresses lower than the proportional limit. Three specific conditions will be considered. First, the case where cracking is assumed to be insignificant will be discussed. In this case, both the fiber and the matrix constituents will be assumed to exhibit creep behaviors, and load sharing will be assumed to exist between the fiber and the matrix. Second, an intermediate case will be considered. In this scenario, significant matrix cracking will be assumed to be present within the

composite even though the composite is loaded lower than the proportional limit. In this scenario, within the slip length region near the matrix crack plane, only the fiber will be assumed to creep. Any load sharing between the fiber and matrix will be assumed to be driven by the interfacial shear stresses between the fiber and the matrix, and the matrix will be assumed to not creep in this region. Beyond the slip length region, both the fiber and matrix will be assumed to creep and load sharing will take place between the fiber and matrix. In the third scenario to be examined in this report, significant matrix cracking will again be assumed to be present. For this case, in the slip length region only the fiber will be assumed to creep. However, in this third scenario, outside of the slip length region the matrix will be assumed to not creep due to the brittle nature of the ceramic matrix. The matrix will be assumed to constrain the fiber such that the fiber will not creep beyond the slip length region. The matrix will be assumed to crack as strain increases, which will place more of the fiber within the slip length region near matrix cracks and thus lead to increased creep in the fiber.

The report will begin with a complete description of the material that was examined, the experimental approach used to obtain the creep data, and a description of how the specific experimental data used in this study was processed. Next, the creep model used to simulate the creep response of the fiber and matrix (as relevant) will be presented, and creep tests on the fiber will be analyzed using the presented creep model. The development of constitutive models to simulate the creep response of the composite will then be discussed for all three matrix cracking scenarios discussed previously. The constitutive model discussion will include the following features of the method. The shear lag-based method used to compute the fiber creep response in the damaged portion of the composite will be discussed. When creep in the portion of the composite outside of the crack/damage region is assumed to take place, the techniques used to compute such creep will be described. The methods used to homogenize the creep response in the regions within and outside of the slip length (to compute the overall composite creep response) will be discussed for the two cases where matrix cracking is assumed to be present. Simulations of the creep response of a representative minicomposite loaded at stresses lower than the proportional limit will be presented. In addition, a detailed description of the effects of including localized matrix cracking in the creep simulations, and the differences in the computed composite creep response resulting from the different scenarios discussed previously will be presented. The ability of the developed model to simulate the creep response of a minicomposite loaded at stresses lower than the proportional limit at a higher fiber volume fraction will also be presented. The overall study represents a detailed examination of the effects of accounting for localized matrix damage in simulating the creep response of ceramic matrix minicomposites, even when they are loaded at stresses lower than the proportional limit. The results of this study should increase the level of understanding of the local material mechanisms that affect the creep response of ceramic matrix composites.

Materials and Experimental Approach

The minicomposite systems that were utilized in this work and the methods used to conduct the experiments are described in this section.

Materials

A SiC_f/SiC minicomposite system was studied in this work. It was manufactured by Rolls-Royce High Temperature Composites, Inc. (Rolls-Royce HTC) (Cypress, CA, USA). The system contains a single Hi-Nicalon Type S™ silicon carbide (SiC) fiber tow manufactured by NGS Advanced Fibers Co., Ltd. (Toyama, Japan), a 0.4 μm chemical-vapor-infiltrated boron nitride (CVI-BN) fiber coating and a silicon carbide (CVI-SiC) matrix. The minicomposites' cross-sectional areas and constituent volume

fractions were computed using the methods described in previous studies (Refs. 4 and 5). Specifically, two specimens with a nominal fiber volume fraction of 0.20 were tested and three specimens with a nominal fiber volume fraction of 0.35 were tested. For the composites with a fiber volume fraction of 0.20, the composite creep stress was approximately 200 MPa. For the specimens with the higher fiber volume fraction, the nominal composite creep stress was approximately 390 MPa. Creep stress on both composites was selected to be slightly less than their matrix cracking stress according to Reference 4. All of the creep tests were conducted at a temperature of 1,200 °C. For each of the specimens, the applied load, composite stress and constituent fiber volume fractions are listed in Table I. The material properties of the constituents are shown in Table II. These properties were obtained from Goldberg, et al. (Ref. 1) and Almansour, et al. (Ref. 5).

Micrographs of a representative minicomposite are shown in Figure 1 (Ref. 12). From the figure, note that the fiber filaments are clustered towards the interior of the cross-section of the composite, and that there is a ring of unreinforced matrix in the exterior of the cross-section. Also note that there is a significant level of porosity in the interior of the composite cross-section.

TABLE I.—SPECIMEN DATA FROM CREEP TESTS

Specimen ID	Composite stress, MPa	Load, N	Fiber volume ratio	Matrix volume ratio	Fiber coating volume ratio
HNSC2-4	251.7	59.9	0.237	0.677	0.086
HNSC3-2	202.5	58.5	0.196	0.734	0.07
HNSC1-1	396.9	60.1	0.373	0.492	0.135
HNSC1-2	365.1	58.5	0.353	0.519	0.128
HNSC1-4	390.3	54.7	0.403	0.451	0.146

TABLE II.—CONSTITUENT DATA FOR MINICOMPOSITES

Property	Values
Fiber radius, μm	6
Average fiber coating thickness, μm	0.4
Fiber density, g/cm^3	3.1
Fiber coating density, g/cm^3	1.5
Matrix density, g/cm^3	3.2
Average crack density at failure, mm^{-1}	1.7
Average crack spacing at failure, mm	0.59
Fiber modulus, GPa	400
Fiber coating modulus, GPa	25
Matrix modulus, GPa	425
Interfacial shear strength, MPa	11
Interfacial debond energy, J/m^2	1.24
Matrix fracture energy, J/m^2	16.7

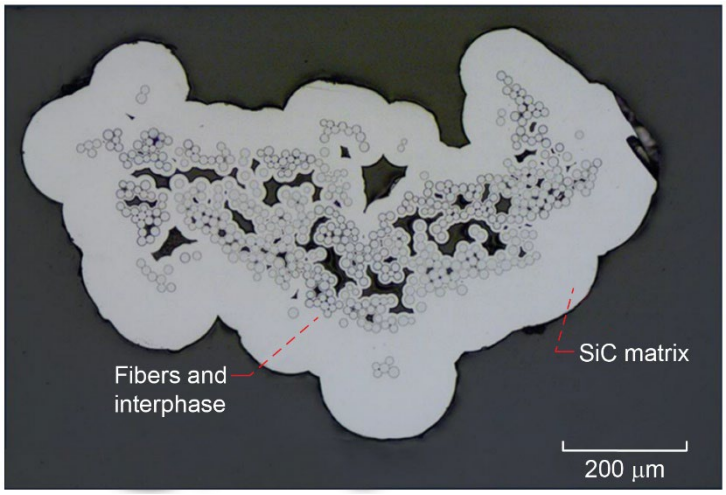

Figure 1.—Representative cross section of SiC_f/SiC minicomposite used in current study.

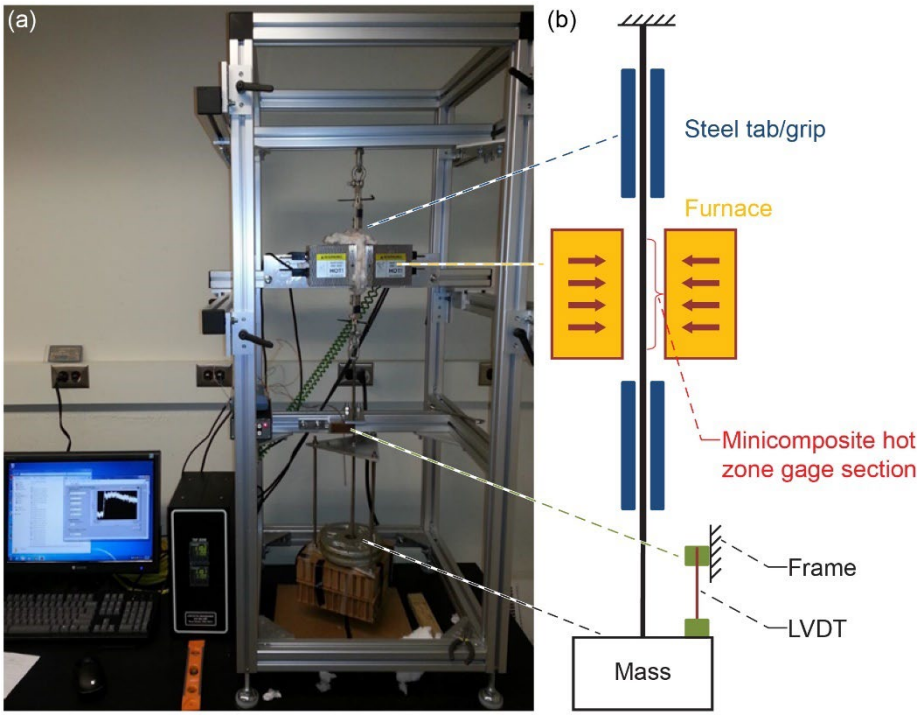

Figure 2.—Experimental setup for creep testing. (a) Creep experiment setup. (b) Schematic of creep experiment.

Experimental Methods

The mounting and preparation of minicomposite creep samples were previously detailed in Almansour, et al. (Ref. 13). Monotonic creep testing of minicomposites was performed at a temperature of 1,200 °C using the creep test setup shown in Figure 2 and the process described in detail in Almansour and Morscher (Ref. 5). The furnace temperature profile throughout the length of the furnace was measured, and the effective gauge length of the minicomposite specimens in the hot zone was calculated, which enabled the computation of engineering strain from the recorded displacement measurements using the procedures described in Almansour and Morscher (Ref. 5). The strain contributions from the thermal

expansion during heating and from room temperature elastic deformation of the sample were deducted from the total strain. The length on both sides of the hot zone at which the temperature drops to room temperature was neglected as described in Almansour and Morscher (Ref. 5). The minicomposite stress was determined by dividing the applied load on the minicomposite by the minicomposite's average cross-sectional area.

Fiber creep data was obtained by testing single Hi-Nicalon-S™ fiber samples in creep at 1,200 °C in vacuum (pressure ~10–4 Pa) using procedures described in Almansour and Morscher (Ref. 5). To obtain approximate matrix data for the CVI-SiC matrix under creep loading conditions, minicomposites with 98 percent CVI-SiC and 2 percent Hi-Nicalon-S™ fibers were tested in creep at 1,200 °C (Ref. 4).

Fiber and Matrix Creep Model

To model the creep behavior of the fiber, a linear Burgers model was utilized. The rheological layout of the model is shown in Figure 3. In the figure, an elastic spring represents the initial elastic response of the material. The spring and dashpot in parallel represent the primary creep and the additional dashpot in series represents the secondary creep.

The creep model represented in the figure can be expressed using Equation (1), where the strain at time t at a particular location "*z*" along the slip length is computed. The stress is assumed to vary along the slip length. In the equation, E_f represents the elastic modulus, E^* represents the spring stiffness in the primary creep regime, η_1 represents the dashpot viscosity in the primary creep regime and η_2 represents the dashpot viscosity in the secondary creep regime. To simplify the characterization of the equation, the η_1/E^* ratio in the primary creep portion of the equation is referred to as a relaxation time τ_r.

$$\varepsilon(z,t) = \frac{\sigma(z)}{E_f} + \frac{\sigma(z)}{E^*}\left[1 - \exp\left(\frac{-E^*}{\eta_1}t\right)\right] + \frac{\sigma(z)}{\eta_2}t$$

$$\tau_r = \frac{\eta_1}{E^*} \tag{1}$$

$$\varepsilon(z,t) = \frac{\sigma(z)}{E_f} + \frac{\sigma(z)}{E^*}\left[1 - \exp\left(\frac{-t}{\tau_r}\right)\right] + \frac{\sigma(z)}{\eta_2}t$$

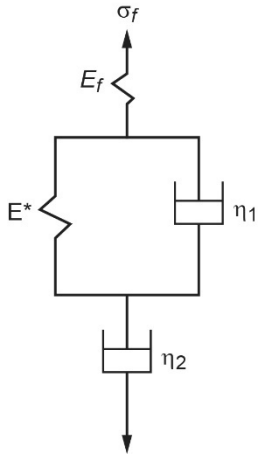

Figure 3.—Rheological schematic of linear Burgers model for creep.

Representative creep curves for Hi-Nicalon-S™ fibers obtained at a temperature of 1,200 °C and stress levels of 204 and 280 MPa are shown in Figure 4. The average slopes of the steady state creep versus time curves were used to obtain a value for η_2. For the remainder of the creep constants, the values used by Almansour and Morscher (Ref. 5) were used as initial values for the constants. The remaining constants were obtained through trial and error by comparing the resulting curves with the measured creep response. This process continued until optimal fits with the creep curves were obtained. The simulated creep curves are also presented in Figure 4, from which it can be observed that a good correlation with the experimental values was obtained. The specific values of the creep constants are listed in Table III.

The inelastic strain versus time curve for the CVI-SiC matrix was obtained at a temperature of 1,200 °C and a constant stress of 69 MPa. The experimental curve is shown in Figure 5. As discussed earlier and in Almansour and Morscher (Ref. 5), these curves were obtained by testing minicomposites with a fiber volume ratio of 0.02. As a result, the obtained curves were assumed to be those of the pure matrix. Almansour and Morscher (Ref. 5) assumed that all of the nonlinearity in the matrix response was due to creep. Assuming that the inelastic response of the matrix is due to creep, the linear Burgers model (Equation (1)) was again used to model the inelastic response of the matrix. The constants for the creep model were adapted from those used by Almansour and Morscher (Ref. 5) and are listed in Table III. The

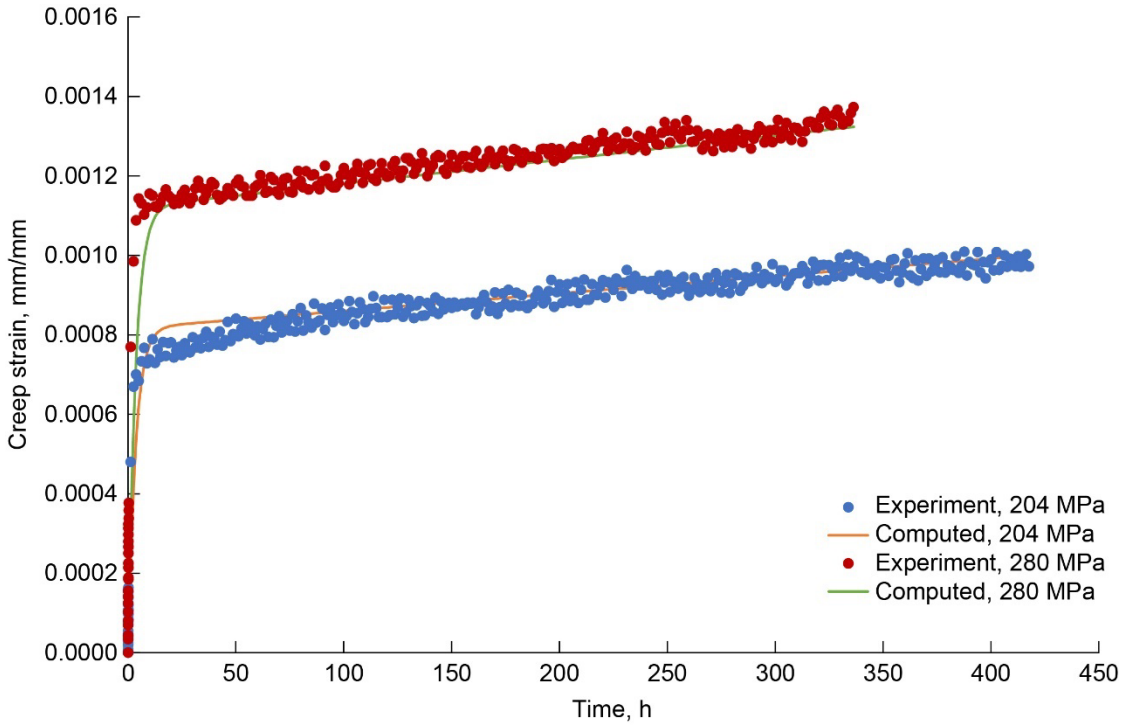

Figure 4.—Experimental and computed creep response of Hi-Nicalon-S™ fibers at 1,200 °C in vacuum.

TABLE III.—CONSTITUENT CREEP MODEL CONSTANTS

Property	Fiber	Matrix
E, Elastic Modulus, GPa	400	425
E^*, Primary Creep Spring Stiffness, MPa	2.5×10^5	3.86×10^4
η_1, Primary Creep Dashpot Viscosity, MPa	3.13×10^9	8.72×10^9
η_2, Secondary Creep Dashpot Viscosity, MPa	1.67×10^{12}	5.52×10^{11}

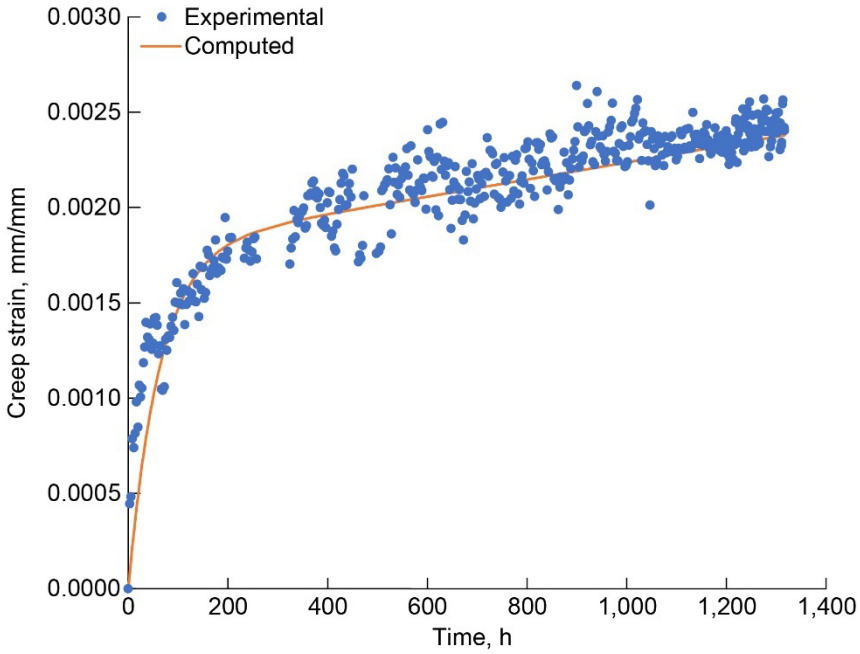

Figure 5.—Experimental and computed creep response for CVI SiC matrix at stress level of 69 MPa and temperature of 1,200 °C. Experimental data obtained from test of SiC_f/SiC composite with fiber volume ratio of 0.02.

correlation between the curves computed by the creep model and the experimental curve is shown in Figure 5. A good correlation was obtained between the experimental and computed results. In the composite analyses to be discussed later in this report, for the cases where the matrix constituent is assumed to creep, Equation (1) and the parameters shown in Table III were used in the analysis. As discussed earlier in this report, due to the relatively high strains observed in the strain versus time curves, at least some of the nonlinearity in the matrix response could be due to the formation and propagation of microcracks in the matrix. The development of an inelastic matrix constitutive model in which the initiation and propagation of cracks will be accounted for will be the subject of future work.

Composite Creep Model

A micromechanics-based method utilizing a shear lag approach in combination with a load sharing approach was employed to simulate the creep response of the composites analyzed in this report.

Overall Assumptions

The fibers in the minicomposites are assumed to be perfectly parallel to each other, have a uniform cross section, and have a uniform BN interface thickness. For these initial studies, a one-dimensional model was developed in which the composite was assumed to be subject to a unidirectional tensile stress, with the transverse normal stresses and the shear stresses assumed to be equal to zero.

As discussed in Goldberg, et al., (Ref. 1) and Swaminathan, et al. (Ref. 2), fast fracture tensile experiments have determined that localized damage is present in minicomposites even when loaded at stresses lower than the proportional limit. An example of a minicomposite loaded at stresses lower than the proportional limit is shown in Figure 6 (Ref. 1), where the matrix cracks are plainly visible. For the composite shown in the figure, the proportional limit was found to be 273 MPa, which is higher than the

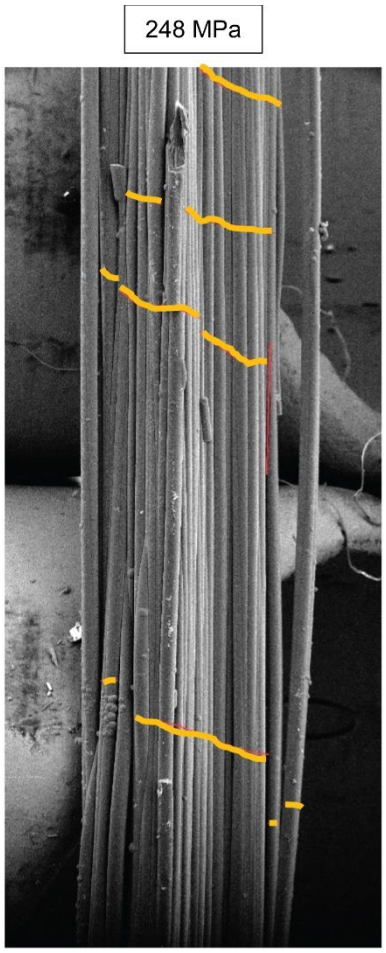

Figure 6.—Micrograph of sample minicomposite loaded in fast fracture loading to stress lower than proportional limit. Note presence of cracks in composite cross section.

stress level at which the micrograph was obtained. As a result, when creep tests are conducted at stress levels lower than the proportional limit, matrix cracking can be assumed to be present in the composite.

In actual minicomposites, as can be seen in Figure 6, matrix cracks have an irregular, disjointed shape. In addition, the cracks are not evenly spaced along the length of the composite cross section. To completely account for the variability in crack width, crack shape, and crack spacing, a full statistical approach would ideally be applied. As a result of the current inability to determine the full statistical distribution of crack shape and crack length, in this study for simplicity the matrix cracks are assumed to be straight and of equal length. Furthermore, because full knowledge of the variability of the crack spacing along the length of the composite cross section is unavailable, the crack spacing along the length of the composite as a function of strain is assumed to be known and constant along the cross-sectional length. In addition, the crack spacing is assigned to be the average crack spacing for each strain level as determined from experimental data obtained from fast fracture testing. The crack spacing data from fast fracture testing was used since relevant crack density versus strain data for minicomposites subjected to creep loading is currently not available. As a result, the crack density evolution with strain is assumed to be identical to that observed under fast fracture loading conditions. Future efforts will endeavor to

develop experimental methods to obtain full statistically distributed data on the damage initiation and growth in the minicomposites of interest, particularly under creep loading conditions. The specific locations of the newly formed cracks are assumed to be random. All of the assumptions discussed previously are assumed to be a highly simplified approximation to the actual geometrical distribution and growth of damage in the composite.

For situations where matrix cracking is assumed to take place, a slip length "*l*" can be defined, which is the distance from a through-thickness crack over which the interfacial shear stress transfers load between the fiber and matrix. Within the slip length region, the fiber creep is assumed to be independent of any creep taking place in the matrix. Furthermore, within the slip length region the stress in the matrix is assumed to not be high enough for matrix creep to occur. Outside of the slip length region, as discussed earlier in this report two conditions will be considered. In the first condition, the matrix will be assumed to undergo creep and the fiber creep will be related to the load sharing between the fiber and matrix as each constituent creeps. In an alternative scenario, outside of the slip length the matrix will be assumed to only undergo cracking and not creep. In this situation, the matrix will be assumed to constrain the fiber such that neither constituent creeps and only elastic straining takes place.

To compute the evolution of the creep strain in the composite, the increment in strain resulting from an increment in time for a condition of constant stress in the composite is computed. For the analysis, the assumption is made that the crack spacing (defined as "2s" in the equations to follow) is constant along the length of each unit cell and equal to the average crack spacing observed experimentally under fast fracture loading conditions for the current value of composite strain. The strains in the fiber, matrix, and composite are assumed to be equal, which is absolutely true at stresses below the proportional limit and approximately true at stresses higher than the proportional limit. As a result, computing the strain in the fiber is assumed to be equivalent to computing the strain in the composite (i.e., $\varepsilon_f = \varepsilon$).

In the equations presented later in this report, the "fiber" properties are assumed to be the synthesized properties of the fiber and fiber coating. The volume fraction ($V_f^{'}$) and modulus ($E_f^{'}$) of the synthesized fiber/coating are computed using a rule of mixtures type of calculation based on the volume fraction and properties of the fiber and coating as shown in Equation (2). Note that, as shown in Table I, for minicomposites the fiber coating has a non-negligible volume fraction such that the coating properties and volume fraction need to be incorporated into the analysis. In Equation (2), the subscript "*i*" indicates values related to the fiber coating and the subscript "*f*" refers to values related to the fiber. This expression implies that the coating doesn't crack and the debonding occurs on the outside of the coating. Experimentally, Lamon et al. (Ref. 14) demonstrated that the debond either occurs on both sides of the coating or a longitudinal crack forms in the middle of the coating. Even though the debond was found to more commonly occur at the fiber/coating interface, the assumption was made for these analyses that only the debond between the coating and matrix was significant. Furthermore, incorporating the fiber and fiber coating into one unit greatly simplified the equation development for the analyses conducted in this study.

$$V_f^{'} = V_f + V_i$$
$$E_f^{'} = \frac{V_f}{V_f^{'}} * E_f + \frac{V_i}{V_f^{'}} * E_i \tag{2}$$

The slip length referred to previously can be defined as a short distance on either side of a matrix crack where the fibers and matrix become debonded and may slip with respect to one another. Slipping is resisted by a shear stress τ acting at the fiber/matrix interface over a slip length "*l*" on either side of the crack plane. As discussed in detail in Goldberg, et al. (Ref. 1) and Sullivan (Ref. 15), the slip length can be computed as shown in Equation (3). In the equation, σ is the far field composite stress, *r* is the fiber

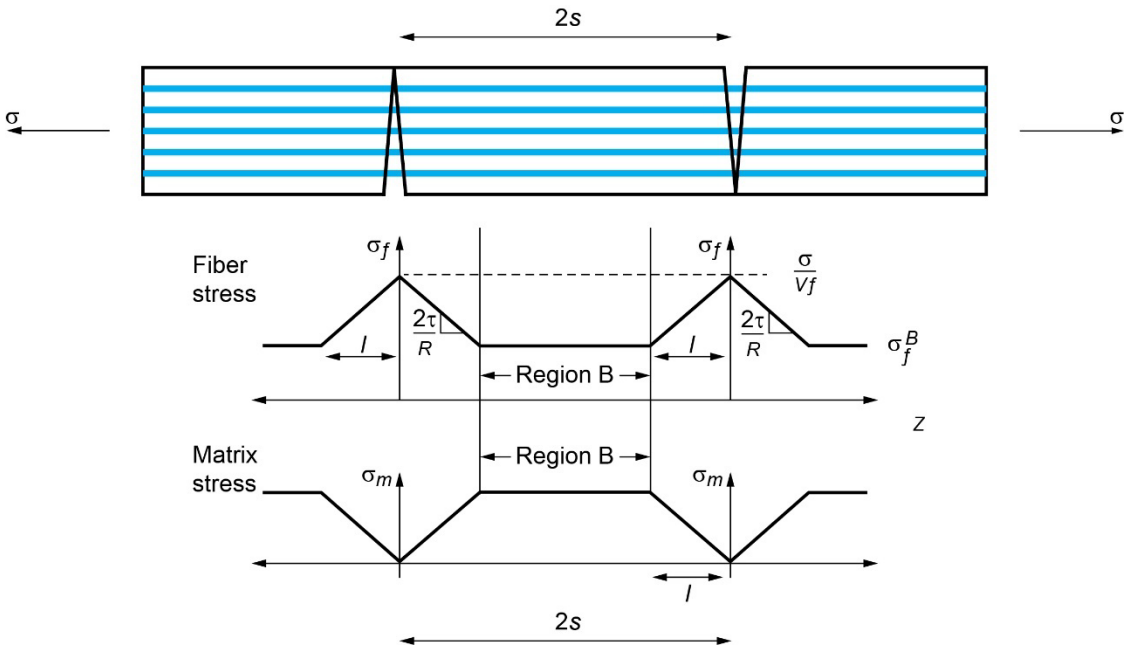

Figure 7.—Stress distribution in fiber in minicomposite under stress σ with two cracks separated by distance 2*s*. Note that intact fibers bridge matrix cracks.

radius, V_f' is the volume fraction of the fiber/coating combination and σ_f^B is the constant fiber stress in the region outside of the slip length (hereafter referred to as Region "*B*" in the composite unit cell as shown in Figure 7).

$$l = \frac{r}{2\tau}\left(\frac{\sigma}{V_f'} - \sigma_f^B\right) \tag{3}$$

The fiber stress is assumed to vary linearly along the slip length as shown in Equation (4). The fiber stress reaches a maximum at the crack plane ($z = 0$), having a value of σ/V_f, decreases over the slip length, and reaches a minimum value of σ_f^B at the end of the slip length ($z = l$). A schematic of the stress distribution within the composite cross section is shown in Figure 7.

$$\sigma_f = \frac{\sigma}{V_f'} - \frac{2\tau z}{r} \tag{4}$$

The value of the fiber stress in the region outside of the slip length (Region "*B*") is dependent on the assumptions made regarding the behavior of the matrix in this region. For the case where the matrix is assumed not to creep, the fiber stress in the continuum stress region is constant and equal to the applied stress multiplied by the ratio of the fiber modulus to the composite modulus. For the case where matrix cracking takes place and the matrix in the continuum stress region outside of the slip length region is also assumed to creep, the fiber stress could be affected by load sharing between fiber and matrix resulting from the creep of both constituents, and the fiber stress in the continuum stress region is assumed to change with time. This concept is summarized in the following paragraphs and is discussed in detail in Almansour and Morscher (Ref. 5).

Following the assumptions made by Rugg, et al. (Ref. 7), the slip length is assumed to remain constant throughout the creep loading process, even when the matrix outside of the slip length region is assumed to creep. However, due to the fact that if matrix creep takes place outside of the slip length the fiber stress in the continuum stress region (Region "*B*") can change with time, to maintain fiber stress continuity at the end of the slip length the effective value of the interfacial shear stress needs to evolve with time, an assumption also made by Rugg, et al. (Ref. 7). The current value of the interfacial stress at any point in time can be expressed by rearranging Equation (3) as shown in Equation (5). Note that in this computation only continuity of the fiber stress between the slip length region and the continuum stress region (Region "*B*") is assured. Discontinuities in the matrix stress at the end of the slip length could occur, which could lead to inaccuracies in the analysis.

$$\tau_{\text{current}} = \frac{r}{2l}\left(\frac{\sigma}{V_f'} - \sigma_f^B\right) \tag{5}$$

As discussed previously, in the current analyses for the cases where matrix cracking is assumed to take place the crack density in the composite is assumed to increase with increasing strain. Furthermore, the evolution of the crack density with strain during creep loading was assumed to be identical to how the crack density evolved with strain during fast fracture loading. Specifically, data obtained by Almansour (Ref. 4) and discussed in Goldberg, et al. (Ref. 1) on the evolution of crack density during fast fracture loading for a SiC/SiC minicomposite with Hi-Nicalon-S™ fibers was utilized. The fiber volume ratio of the fast fracture specimens was slightly higher than the specimens used for the creep studies discussed in this study (0.22 for the fast fracture specimens as opposed to 0.20 for the creep specimens), but the results obtained from the fast fracture studies were assumed to be valid for the analyses conducted here. A graph of the evolution of crack density with strain obtained from the fast fracture tests described prevously is presented in Figure 8. The reciprocal of the crack density function was used to compute the current value of the crack spacing at a particular strain level for the creep strain calculations. The crack spacing and its evolution with strain was assumed to be a known input to the composite creep model.

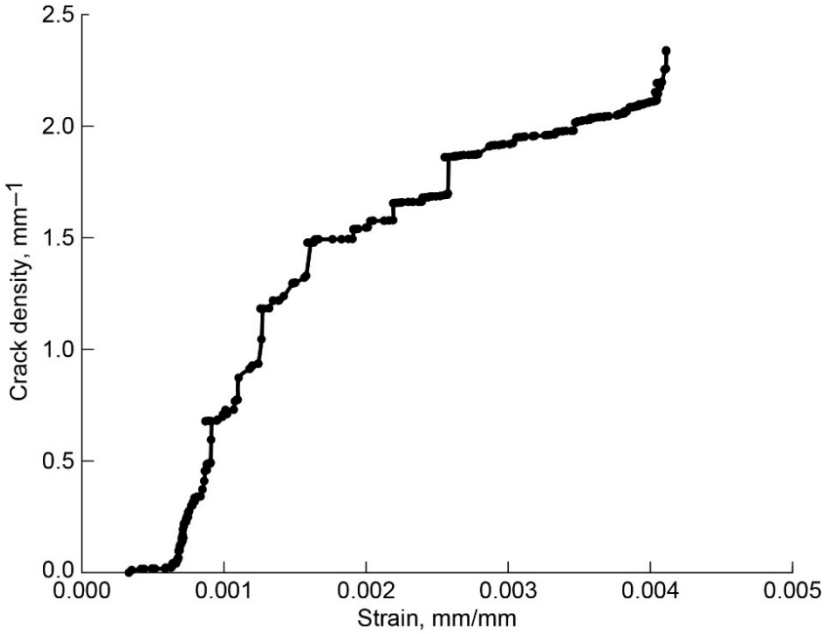

Figure 8.—Variation of crack density with strain for minicomposite subjected to fast fracture loading. Data obtained from Almansour, et al. (Ref. 4).

Computation of Fiber Creep Strain

To compute the overall creep strain in the composite at a particular time step, the creep strain in the fiber is determined. Due to the isostrain assumptions the strain in the fiber is assumed to be equal to the strain in the composite. As discussed earlier, three sets of assumptions regarding matrix cracking and matrix creep were considered in the development of methods to compute the fiber (and thus the composite) creep. A set of analyses were carried out applying each of these three conditions. The three sets of assumptions are summarized in Table IV. For the first set of analyses, hereafter referred to as "Assumption 1", matrix microcracking was assumed to be insignificant, and the fiber and matrix were both assumed to creep. All of the nonlinearity in the matrix was assumed to be due to creep and not localized cracking.

Due to the fact that creep is a time dependent and path dependent phenomena, for this case with no matrix cracking and combined fiber and matrix creep, an incremental approach was employed. To compute the creep strain at time $t+\Delta t$, a rate-based forward Euler approach was used (Ref. 16). In this approach, as is shown in Equation (6), the creep strain rate at time t is computed, and the creep strain rate is used along with creep strain at time t to compute the strain at time $t+\Delta t$. In the equation, the superscript "*C*" specifies that the strains are the creep strains. Note that this is equivalent to a time hardening rule in classical creep analysis (Ref. 17). While a strain hardening rule can be more accurate, very small time steps were used such that the time hardening rule was deemed to be sufficiently accurate. By using this approach, the equation development was simplified and the need for an iteration algorithm was avoided.

$$\varepsilon^C\left(t+\Delta t\right)=\dot{\varepsilon}^C\Delta t+\varepsilon^C\left(t\right) \tag{6}$$

To compute the creep strain rate in the composite, the approach for creep strain calculations developed by Almansour and Morscher (Ref. 4) was modified. First, the strain in the fiber and matrix are determined by applying Equation (1) for each of the constituents. The resulting expressions are shown in Equation (7). In the equation, the subscript "*f*" refers to fiber related quantities and the subscript "*m*" refers to matrix related quantities.

$$\begin{aligned}\varepsilon_f&=\frac{\sigma_f}{E_f^{'}}+\frac{\sigma_f}{E_f^*}\left[1-\exp\left(\frac{-t}{\tau_{rf}}\right)\right]+\frac{\sigma_f}{\eta_{2f}}t\\ \varepsilon_m&=\frac{\sigma_m}{E_m}+\frac{\sigma_m}{E_m^*}\left[1-\exp\left(\frac{-t}{\tau_{rm}}\right)\right]+\frac{\sigma_m}{\eta_{2m}}t\end{aligned} \tag{7}$$

The time derivatives of the expressions in Equation (7) are then taken to determine the strain rates of the fiber and matrix, as shown in Equation (8).

$$\begin{aligned}\dot{\varepsilon}_f&=\frac{\dot{\sigma}_f}{E_f^{'}}+\frac{\dot{\sigma}_f}{E_f^*}\left[1-\exp\left(\frac{-t}{\tau_{rf}}\right)\right]+\frac{\dot{\sigma}_f}{\eta_{2f}}t+\frac{\sigma_f}{E_f^*}\left[\frac{1}{\tau_{rf}}\exp\left(\frac{-t}{\tau_{rf}}\right)\right]+\frac{\sigma_f}{\eta_{2f}}\\ \dot{\varepsilon}_m&=\frac{\dot{\sigma}_m}{E_m}+\frac{\dot{\sigma}_m}{E_m^*}\left[1-\exp\left(\frac{-t}{\tau_{rm}}\right)\right]+\frac{\dot{\sigma}_m}{\eta_{2m}}t+\frac{\sigma_m}{E_m^*}\left[\frac{1}{\tau_{rm}}\exp\left(\frac{-t}{\tau_{rm}}\right)\right]+\frac{\sigma_m}{\eta_{2m}}\end{aligned} \tag{8}$$

TABLE IV.—LIST OF ASSUMPTIONS USED IN CREEP ANALYSES

Assumption number	Matrix cracking	Fiber creep in slip length	Fiber and matrix creep outside of slip length
1	No	N/A	Yes
2	Yes	Yes	Yes
3	Yes	Yes	No

Due to the isostrain assumption that the strain (and strain rate) in the fiber equals the strain (and strain rate) in the matrix, the two expressions in Equation (8) can be set equal to each other. The stress rate in the fiber can then be solved for. The first step in solving for the fiber stress rate is to use the rule of mixtures to express the stress and stress rate of the matrix in terms of the stress and stress rate of the fiber, as shown in Equation (9). Note that the total stress rate for the composite is set equal to zero due to the fact that creep is conducted under constant stress conditions.

$$\begin{aligned} \dot{\sigma} = 0 &= V_f' \dot{\sigma}_f + \left(1 - V_f'\right)\dot{\sigma}_m \\ \dot{\sigma}_m &= \frac{-V_f'}{\left(1 - V_f'\right)}\dot{\sigma}_f \\ \sigma &= V_f' \sigma_f + \left(1 - V_f'\right)\sigma_m \\ \sigma_m &= \frac{\sigma - V_f' \sigma_f}{\left(1 - V_f'\right)} \end{aligned} \tag{9}$$

By substituting Equation (9) into Equation (8), the fiber stress rate in the composite can be found to be represented by the expression shown in Equation (10). As also shown in Equation (11), a forward Euler method can then be used to compute the stress in the fiber at time $t+\Delta t$.

$$\dot{\sigma}_f = \frac{\left(\frac{\sigma - V_f' \sigma_f}{1 - V_f'}\right)\left[\frac{1}{E_m^*}\frac{1}{\tau_{rm}}\exp\left(\frac{-t}{\tau_{rm}}\right) + \frac{1}{\eta_{2m}}\right] - \sigma_f\left[\left[\frac{1}{E_f^*}\frac{1}{\tau_{rf}}\exp\left(\frac{-t}{\tau_{rf}}\right) + \frac{1}{\eta_{2f}}\right]\right]}{\frac{1}{E_f'} + \frac{1}{E_f^*}\left[1 - \exp\left(\frac{-t}{\tau_{rf}}\right)\right] + \frac{1}{\eta_{2f}}t + \left(\frac{V_f'}{1 - V_f'}\right)\left(\frac{1}{E_m} + \frac{1}{E_m^*}\left[1 - \exp\left(\frac{-t}{\tau_{rm}}\right)\right] + \frac{t}{\eta_{2m}}\right)} \tag{10}$$

$$\sigma_f\left(t + \Delta t\right) = \dot{\sigma}_f \Delta t + \sigma_f(t) \tag{11}$$

The stress (and stress rate) of the fiber is then used to compute the creep strain rate of the fiber by substituting Equations (10) and (11) into Equation (8), as shown in Equation (12). Note that in this equation the elastic strain rate has been subtracted out to yield only the creep strain rate. Using the forward Euler integration approach (Ref. 16), the creep strain in the fiber at time $t+\Delta t$ can also be computed based on the creep strain rate as shown in Equation (13).

$$\dot{\varepsilon}^C = \left[\dot{\sigma}_f\left(\frac{1}{E_f'} + \frac{1}{E_f^*}\left[1 - \exp\left(\frac{-t}{\tau_r^f}\right)\right] + \frac{t}{\eta_{2f}}\right) + \sigma_f^B\left[\frac{1}{E_f^*}\frac{1}{\tau_r^f}\exp\left(\frac{-t}{\tau_r^f}\right) + \frac{1}{\eta_{2f}}\right]\right] - \frac{\dot{\sigma}_f}{E_f'} \tag{12}$$

$$\varepsilon^C\left(t + \Delta t\right) = \dot{\varepsilon}^C \Delta t + \varepsilon^C(t) \tag{13}$$

The second set of assumptions considered for this study, as specified in "Assumption 2" in Table IV, include the possibility that cracking occurs in the matrix while creep loading is applied. Under this

assumption, outside of the slip length both the fiber and matrix are assumed to creep and the equations presented previously are used to compute the creep strain in this region (Region "*B*" as defined in Figure 7). Within the slip length region (referred to as Region "*A*" in the equations that follow and is the region of varying fiber stress in Figure 7), the creep strain rate of the fiber (and thus the composite) is computed using the equations that follow. A volume averaging process is then used to obtain the overall composite creep strain.

To compute the creep strain rate in the slip length region, as shown in Equation (14), first, the total fiber displacement u_A within the slip length region is determined by integrating the fiber creep strain (Equation (1)) over the slip length, where the current fiber stress at the particular location along the slip length (Equation (4)) is substituted in for the stress term. In the equation, z is the coordinate along the length of the fiber, the subscript "*f*" indicates that the properties of the fibers are to be used, and the remaining terms are as defined previously. Note that the value of the interfacial shear stress τ is the current value of this parameter as defined in Equation (5).

$$u_A = \int_0^l \left(\frac{\sigma}{V_f} - \frac{2\tau_{\text{curr}} z}{r} \right) \left[\frac{1}{E_f} + \frac{1}{E_f^*} \left(1 - \exp\left(\frac{-t}{\tau_{rf}} \right) \right) + \frac{t}{\eta_{2f}} \right] dz$$
$$u_A = \left[\frac{1}{E_f} + \frac{1}{E_f^*} \left(1 - \exp\left(\frac{-t}{\tau_{rf}} \right) \right) + \frac{t}{\eta_{2f}} \right] \left(\frac{\sigma l}{V_f} - \frac{\tau_{\text{curr}} l^2}{r} \right) \tag{14}$$

To compute the total strain in the slip length region, as shown in Equation (15) the displacement is divided by the slip length.

$$\varepsilon_A = \left[\frac{1}{E_f} + \frac{1}{E_f^*} \left(1 - \exp\left(\frac{-t}{\tau_{rf}} \right) \right) + \frac{t}{\eta_{2f}} \right] \left(\frac{\sigma}{V_f} - \frac{\tau_{\text{curr}} l}{r} \right) \tag{15}$$

To compute the creep strain rate, the derivative of the total strain with respect to time is determined as shown in Equation (16). Note that since the elastic strain is not time dependent, the derivative of this term with respect to time is equal to zero, which results in only the creep strain rate being computed. Since the slip length is assumed to remain constant with time, the derivative of this term with time was assumed to be equal to zero. Any effects of the rate of change of the interfacial shear stress with time were neglected to simplify the calculations. These effects were assumed to be implicitly accounted for by the variation of the stress in the area outside of the slip length region. However, this assumption could lead to an underprediction of the creep strain in the slip length region.

$$\dot{\varepsilon}_A^C = \left(\frac{\sigma}{V_f} - \frac{\tau_{\text{curr}} l}{r} \right) \left[\left[\frac{1}{E_f^*} \frac{1}{\tau_r^f} \exp\left(\frac{-t}{\tau_r^f} \right) + \frac{1}{\eta_{2f}} \right] \right] \tag{16}$$

To compute the creep strain for the current time increment in the slip length region, a forward Euler type of calculation is used.

$$\varepsilon_A^C (t + \Delta t) = \dot{\varepsilon}_A^C \Delta t + \varepsilon_A^C (t) \tag{17}$$

To compute the creep strain in the overall composite, the volume average of the creep strain in the fiber in the slip length region and the creep strain in the fiber in the region outside of the slip length is volume averaged. The unit cell for these analyses is assumed to extend from the crack plane to half of the

distance to the next crack (s). The volume averaging expression is shown in Equation (18), where "s" is one-half of the crack spacing.

$$\varepsilon^C(t+\Delta t) = \frac{l}{s}\varepsilon_A^C(t+\Delta t) + \left(1-\frac{l}{s}\right)\varepsilon_B^C(t+\Delta t) \tag{18}$$

For the third set of assumptions examined in this study, as defined in the listing for "Assumption 3" in Table IV, matrix cracking was again assumed to occur, and the fiber within the slip length region was assumed to creep. However, the creep of both the fiber and matrix in the region outside of the slip length region was assumed to be negligible, and the fiber stress in the region outside of the slip length was assumed to remain at its initial value, specified as the product of the applied stress and the ratio of the composite modulus to the fiber modulus.

Due to the fact that only the fiber creep in the slip length region is computed using this set of assumptions, a rate approach was not applied and the fiber creep strain in the slip length region for each time step was directly computed using Equation (15). Note that since the fiber stress outside of the slip length region (Region "*B*") was assumed to remain constant with time, the interfacial shear stress remained constant at its initial value. The fiber creep strain for the composite was then computed using Equation (18), where the creep strain in the region outside of the slip length (Region "*B*") was assumed to be zero.

Analysis Results

To carry out the simulations of the creep response of the material, the equations and algorithm described previously were programmed into a MATLAB® (The MathWorks, Inc.) routine. Representative tests from the test series shown in Table I were analyzed here, as opposed to attempting to create an average curve to represent the variability in the experimental results. The nominal material properties for the fiber, matrix, and interface that were employed in this study are those listed in Table II and Table III. First, the specimen 3-2 shown in Table I (with a nominal fiber volume ratio of 0.196) was analyzed. As shown in Table I, the applied creep stress was 202.5 MPa, which is lower than the nominal proportional limit, and the test was conducted at a temperature of 1,200 °C.

For the two cases where matrix cracking was assumed to be present in the minicomposite ("Assumption 2" and "Asssumption 3" as defined in Table IV), the variation of the crack spacing with total strain was developed based on the crack density versus strain curve shown in Figure 8, which as discussed earlier was generated from a fast fracture loading test at room temperature of a minicomposite with an equivalent fiber volume ratio. For the approach where creep was assumed to take place both within and outside of the slip length region ("Assumption 2"), a curve fit of the entire curve shown in the figure was conducted to determine the variation of crack spacing as a function of strain. Since this approach is an incremental, history dependent analysis method, the assumption was made that having a best fit expression for the crack density evolution over the entire strain range shown in the curve would provide improved results. The crack spacing evolution equation (in millimeters) as a function of strain was defined as shown in Equation (19).

$$2s = 1/\left[1.1384\ln(\varepsilon) + 3.2666\right] \tag{19}$$

For the approach where matrix cracking was present and creep was assumed to only take place within the slip length region ("Assumption 3" as defined in Table IV), a curve fit was only conducted on an approximately linear portion of the crack density versus strain curve shown in Figure 8. This linear region

consisted of the portion of the curve between approximately 1.2 percent strain and 1.8 percent strain, the key strain range where creep takes place. Since this approach is a non-incremental approach, which just uses the current values of stress, time and crack density, the assumption was made that having the most accurate curve fit possible for the strain range of key interest was most critical. While the crack density at low strain levels could be overpredicted using this approach, the desire to obtain a more accurate curve fit in the critical strain regions was desired. The average linear curve fit for the variation of crack spacing as a function of strain is given in Equation (20).

$$2s = 1/[631.08 * \varepsilon + 0.3347] \tag{20}$$

The experimental and simulated creep strain versus time curves for Specimen 3-2 are shown in Figure 9. The test was conducted at 1,200 °C. The fiber volume ratio was 0.20 and the tests were conducted at a stress level of approximately 200 MPa. The curve labeled "No Matrix Cracking" was generated for the case that assumed that there was no cracking in the composite (Assumption 1), and the fiber and matrix were assumed to creep simultaneously over the entire length of the composite. As discussed earlier, this is the assumption that was made in the study conducted by Almansour and Morscher (Ref. 5). As can be seen in the figure, the simulated creep response was underpredicted as compared to the experimental curve over the entire creep time. These results are consistent with what was obtained by Almansour and Morscher (Ref. 5). The curve labeled "Matrix Cracking-Creep Full Composite" was generated by assuming that cracking was present in the composite and there was a slip length region (Assumption 2). These calculations were conducted by computing the fiber creep in the slip length region and the simultaneous fiber and matrix creep in the region outside of the slip length. These calculations predicted higher creep strains, which more accurately correlated to the experimental results over the entire creep time. The case where matrix cracking was again assumed to be present but with

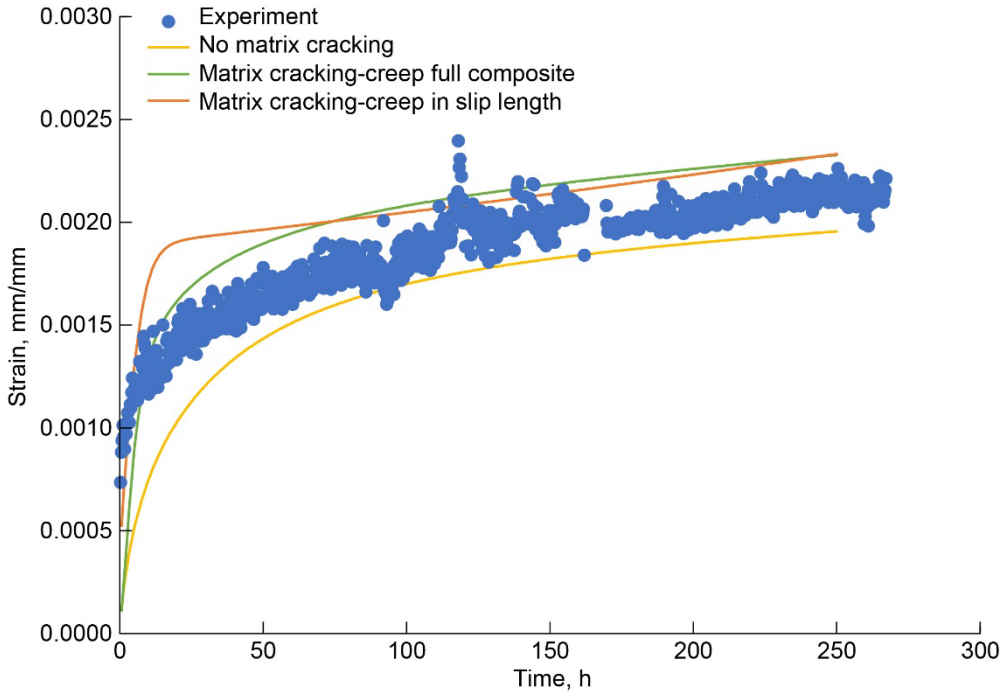

Figure 9.—Experimental and computed creep strain versus time curves for minicomposites with fiber volume fraction of 0.20 with variety of assumptions relating to presence of matrix cracking and scope of creep in composite. Creep took place at temperature of 1,200 °C at stress level of 200 MPa.

creep assumed to only take place in the fiber within the slip length (Assumption 3) was also simulated. The creep curve computed by using this assumption is also plotted in Figure 9 and is labeled "Matrix Cracking-Creep in Slip Length" in the figure. The creep curve for this condition is more of a bi-linear curve compared to the previous results, which had a more gradual variation of the creep strain as a function of time. This bi-linear curve most likely resulted from the linear variation of the crack density with strain that was assumed for these computations. The creep curve computed using these assumptions also provided a good correlation to the experimental results, particularly at higher creep times. The creep curves predicted for this third case overpredicted the experimental results at lower creep times. The cause of this discrepancy is most likely due to the simple linear variation of the crack density with time, which was assumed for this case. The crack density was dynamically varied during the analysis based on the level of total strain. At lower strain levels the crack density was likely overpredicted by the curve fit, which would be reflected in the creep predictions at lower creep times. This discrepancy will be further examined in future work.

The overall conclusion to be drawn from the results shown in Figure 9 is that assuming that matrix cracking takes place during creep results in greatly improved correlations of the simulations with the experimental results. These results strongly indicate that even though the composite creep was conducted at a stress level lower than the proportional limit, matrix cracking was likely present and strongly affecting the creep response. The fact that the curve predicted by assuming that creep only takes place in the slip length region (and only in the fiber in the slip length region) provides a reasonable correlation to the experimental results provides additional support to this conclusion. Future work will involve conducting detailed experimental studies in which creep studies will be conducted on relevant minicomposites with acoustic emission techniques to explore in detail the extent of matrix cracking that takes place during a creep test. In addition, interrupted tests will be conducted and scanning electron microscope imaging will be used to further explore the extent of cracking that is present. These studies should provide further insight and confirmation of the conclusions reached in this analytical study.

To further explore the concept of matrix cracking not only being present but evolving during the process of creep loading, the variation of the ratio of the slip length to one-half the crack spacing (referred to as the "l/s ratio") as creep progresses was investigated. Figure 10 shows the variation of the "l/s ratio" as a function of creep time for the case where matrix cracking is present and simultaneous creep takes place both within and outside of the slip length (Assumption 2). The experimental and computed creep versus time curves are also plotted for comparison. As can be seen in the figure, the "l/s ratio" rapidly evolves with time and reaches a maximum value of approximately 0.6, indicating that the slip length region occupies over half of the length of the composite unit cell. These results indicate that not only is significant localized cracking likely present, but the crack density noticeably increases with time. These results are reasonable since with the matrix being a brittle material, even with a constant applied composite stress strain increases could lead to additional matrix cracking. The shape of the creep versus time curve also is qualitatively very similar to the variation of the l/s ratio with time, providing further confirmation of the effects of matrix cracking and its growth on the creep response. The cause of this close similarity between the shape of the creep curve and the curve showing the variation of the l/s ratio with time needs to be investigated further in future work. Similar results are seen in Figure 11, which displays the same types of results for the case where creep is only assumed to take place in the portion of the fiber located within the slip length (Assumption 3). For this case, the maximum l/s ratio is equal to approximately 0.8, indicating that most of the composite unit cell is within the slip length. As discussed earlier, focused experimental studies need to be conducted to examine the extent of matrix cracking that is present in actual specimens that are subject to creep at stress levels lower than the proportional limit.

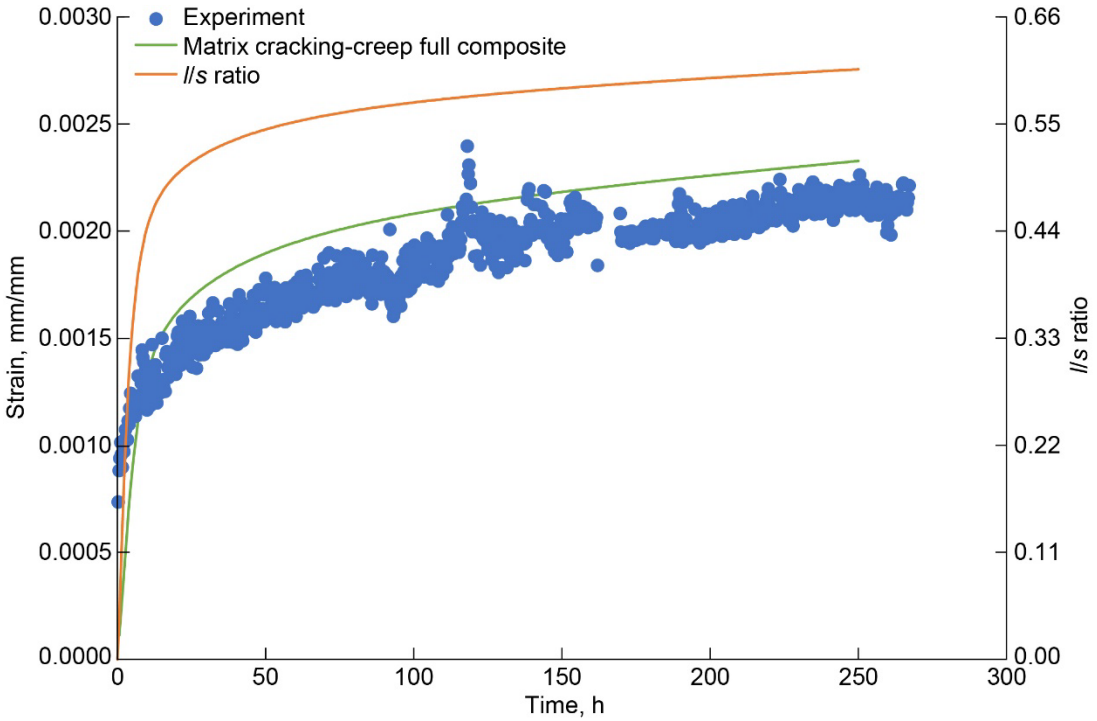

Figure 10.—Variation of ratio of slip length to half crack spacing (*l*/*s* ratio) with time for a minicomposite with fiber volume fraction of 0.20 assuming creep takes place both within and outside of slip length. Experimental and computed creep strain versus time curves included for comparison. Creep took place at temperature of 1,200 °C at stress level of 200 MPa.

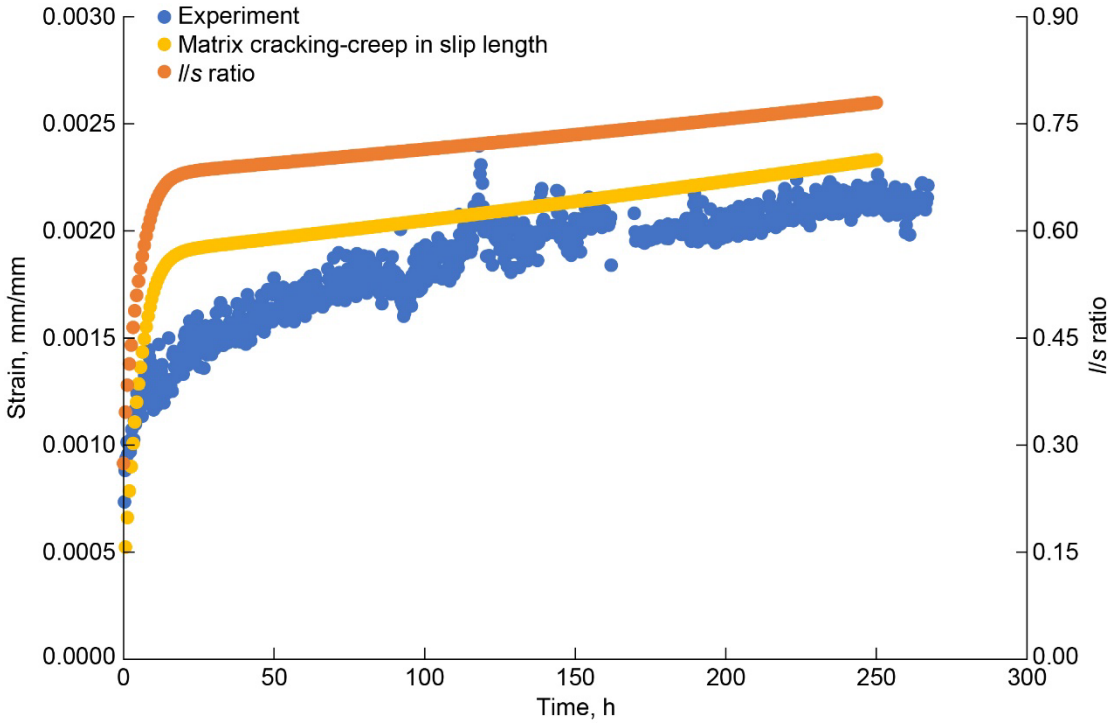

Figure 11.—Variation of ratio of slip length to half crack spacing (*l*/*s* ratio) with time for minicomposite with fiber volume fraction of 0.20 assuming creep takes place only within slip length. Experimental and computed creep strain versus time curves included for comparison. Creep took place at temperature of 1,200 °C at a stress level of 200 MPa.

This testing will involve a combination of acoustic emission measurements and interrupted creep tests where the initiation and growth of cracks in actual specimens can be examined in detail.

To further explore the effects of matrix damage on the creep response of minicomposites, and to examine the effects of the fiber volume ratio on the creep response, Case 1-1 from Table I was analyzed. In this test, the fiber volume ratio was 0.373, the applied creep stress was 400 MPa and the temperature was again 1,200 °C. Lacking appropriate experimental data, the crack density evolution as a function of strain based on the curve shown in Figure 8, obtained from a room temperature fast fracture test of a composite with a fiber volume ratio of 0.20, was utilized. While the crack density evolution shown in Figure 8 is almost certainly different from what took place in the creep test under consideration, due to both the difference in test type and the difference in fiber volume ratio, for the initial conceptual study described in this work the values were assumed to be acceptable and approximately correct. As can be seen in Figure 12, the simulated curve generated assuming that no matrix damage was present (Assumption 1-labeled “No Matrix Cracking”) again underpredicted the experimental creep results. By incorporating the effects of matrix damage, for the case where creep was assumed to take place both within and outside of the slip length (Assumption 2), the creep curve generated using this set of assumptions (labeled “Matrix Cracking-Creep Full Composite” in the figure) resulted in an improved correlation with the experimental results, but an underprediction of the experimental creep curve at higher creep times. For the case where creep was assumed to only take place within the slip length (Assumption 3-labeled “Matrix Cracking-Creep in Slip Length” in the figure), the simulated creep curve provided an improved correlation to the experimental results at higher creep times, but overpredicted the experimental results earlier in the creep process. The causes for the discrepancies between the experimental and the simulated results observed for the cases where matrix damage was assumed to be present in the composite

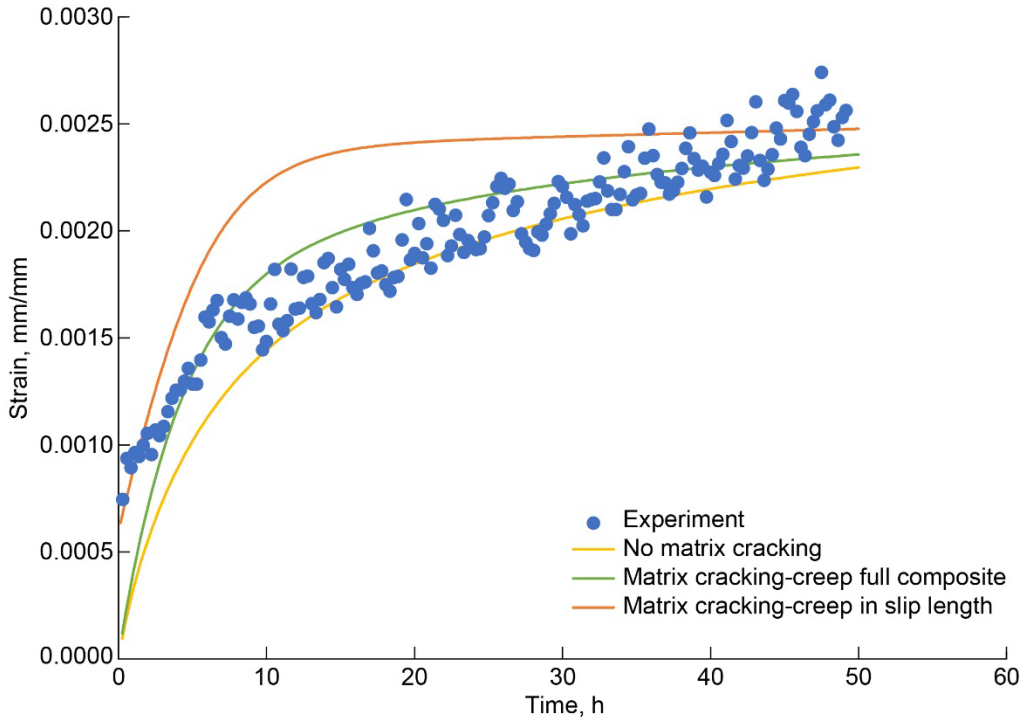

Figure 12.—Experimental and computed creep strain versus time plots for minicomposite with fiber volume fraction of 0.373 with variety of assumptions relating to presence of matrix cracking and scope of creep in the composite. Creep took place at temperature of 1,200 °C at stress level of 400 MPa.

were likely due to the assumptions that were made regarding the evolution of crack density with strain. Specifically, the curve fit equations and assumptions used to compute the dynamically varying crack density with increasing strain were likely a significant contributor to the differences between the experimental and analytical results. Future experimental efforts will endeavor to obtain actual measurements of the change in crack spacing in a composite during creep loading. Even with the discrepancies, however, the obtained results indicate that accounting for the matrix damage that takes place during creep loading leads to improved predictions of the composite creep response.

In Figure 13 and Figure 14, the effects of the matrix damage and cracking for the higher volume fraction case are explored in greater depth. Figure 13 shows the variation of slip length to one-half of the crack spacing ("*l*/*s* ratio") for the case where creep was assumed to take place both within and outside of the slip length, and Figure 14 shows the variation of the *l*/*s* ratio with time for the case where creep was assumed to only take place within the slip length. For both cases, similar to what was observed for the lower fiber volume ratio case, the *l*/*s* ratio increased significantly with time and approached an asymptotic value of around 0.5 for the case where creep was assumed to take place both within and outside of the slip length and an asymptotic of around 0.85 for the case where creep was assumed to only take place in the slip length. This variation of the maximum *l*/*s* ratio for the two cases is related to the fact that when the matrix is assumed to creep outside of the slip length the magnitude of the shear stress varies and is different from the other case. These results indicate that for this higher fiber volume ratio case the slip length region also formed a significant percentage of the length of the composite unit cell. Similar to what was observed for the lower fiber volume ratio case, the shape of the *l*/*s* ratio versus time curves correlated very closely with the predicted creep curves, for reasons that need to be investigated further in future work. Overall, however, these results further demonstrate that matrix damage and the creep response in the slip length region significantly effects the creep response of the composite.

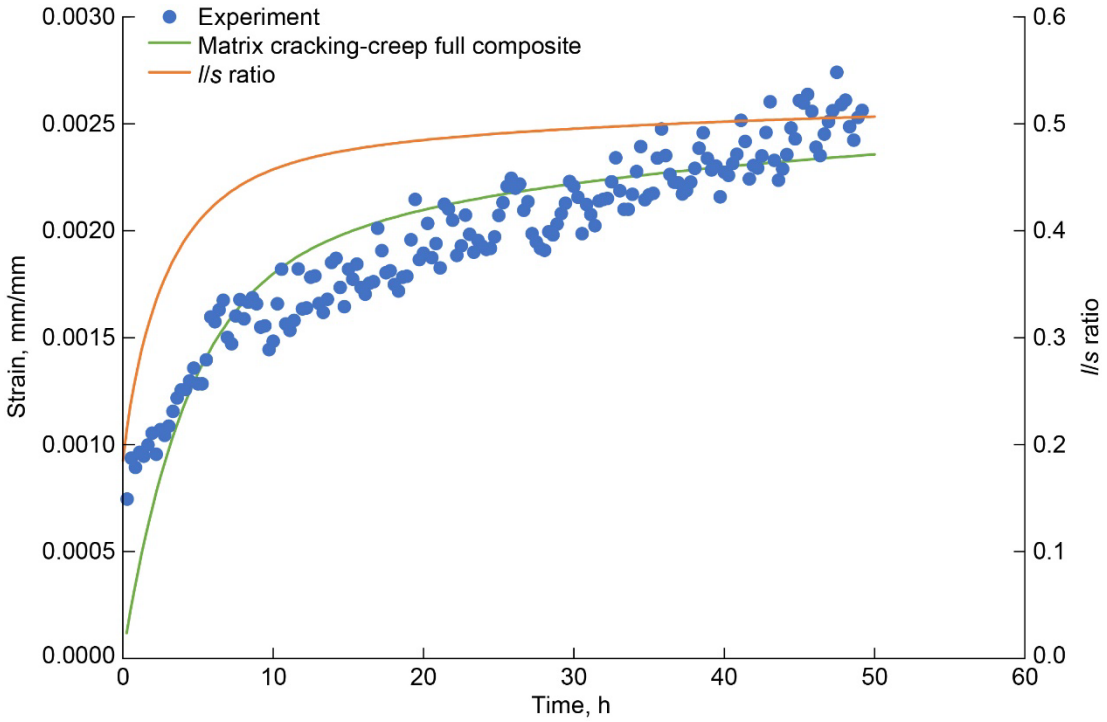

Figure 13.—Variation of ratio of slip length to half crack spacing (*l*/*s* ratio) with time for minicomposite with fiber volume fraction of 0.373 assuming creep takes place both within and outside of slip length. Experimental and computed creep strain versus time curves included for comparison. Creep took place at temperature of 1,200 °C at stress level of 400 MPa.

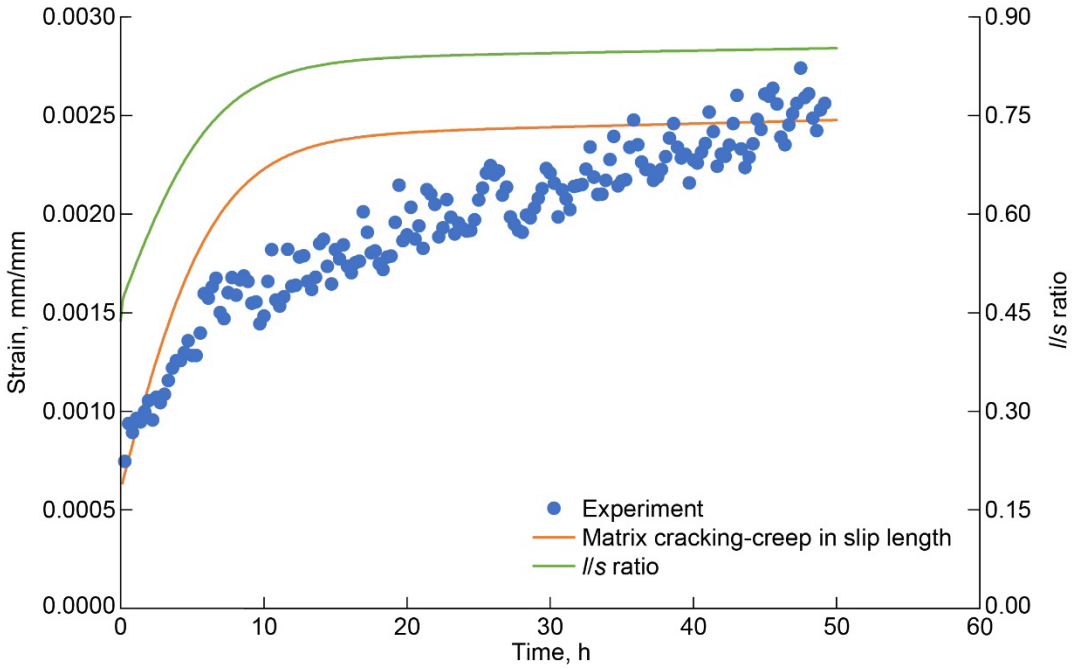

Figure 14.—Variation of ratio of slip length to half crack spacing (*l*/*s* ratio) with time for minicomposite with fiber volume fraction of 0.373 assuming creep takes place only within slip length. Experimental and computed creep strain versus time curves included for comparison. Creep took place at temperature of 1,200 °C at stress level of 400 MPa.

Conclusions

A methodology has been developed to simulate the creep response of SiC/SiC minicomposites which accounts for effects of localized damage. To conduct the analyses, a shear lag-based model was utilized to compute the creep response in the damaged region of the composite unit cell. Volume averaging techniques were used to compute the creep response of the overall minicomposite. Various sets of assumptions regarding the presence of matrix damage in the composite and the presence of creep both within and outside of the damaged region of the composite were investigated.

By incorporating the localized matrix damage into the creep analyses, an improved correlation with experimental creep curves was obtained, compared to simulations which were conducted in which no localized damage was assumed to be present. The creep in the region of the composite assumed to contain matrix cracks was found to be a significant contributor to overall composite creep response. The results obtained in this report provide a preliminary indication that even when ceramic matrix composites are subjected to creep at stress levels lower than the proportional limit, localized matrix damage may still significantly affect the creep response of the composite and should be accounted for in the design and analysis of structures composed of these materials. Future efforts will involve conducting detailed experimental studies to specifically investigate the initiation and progression of matrix damage in ceramic matrix composites subjected to creep loading. The results from these types of studies will be used to modify the analysis methods. Future efforts will also involve expanding the scope of the analyses to examine creep in macrocomposites.

References

1. Goldberg, R.K; Almansour, A.S.; and Sullivan, R.M.: Analytical Simulation of Effects of Local Mechanisms on Tensile Response of Ceramic Matrix Minicomposites. NASA TM-20210012652, 2021. https://ntrs.nasa.gov
2. Swaminathan, B., McCarthy, N.R., Almansour, A.S., Sevener, K., Pollock, T.M., Kiser, J.D. and Daly, S. 2020. Microscale characterization of damage accumulation in CMCs. Journal of the European Ceramic Society, vol. 41, pp. 3082–3093.
3. Bhatt, R.T.; and Kiser, J.D.: Creep behavior and failure mechanisms of CVI and PIP SiC/SiC composites at temperatures to 1650 °C in air. J. Eur. Ceram. Soc., vol. 41, 2021, pp. 6196–6206.
4. Almansour, A., et al.: Effect of Fiber Content on Single Tow SiC Minicomposite Mechanical and Damage Properties Using Acoustic Emission. J. Eur. Ceram. Soc., vol. 35, no. 13, 2015, pp. 3389–3399.
5. Almansour, A.S.; and Morscher, G.N.: Tensile Creep Behavior of SiC_f/SiC Ceramic Matrix Minicomposites. J. Eur. Ceram. Soc., vol. 40, no. 15, 2020, pp. 5132–5146.
6. Sauder, C.; and Lamon, J.: Creep behavior and failure mechanisms of CVI and PIP SiC/SiC composites at temperatures to 1650 °C in air. J. Am. Ceram. Soc., vol. 90, no. 4, 2007, pp. 1146–1156.
7. Rugg, K.L.; Tressler, R.E.; Bakis, C.E.; and Lamon, J.: Creep of SiC/SiC Microcomposites. J. Eur. Ceram. Soc., vol. 19, 1999, pp. 2285–2296.
8. Mital, S.K.; Arnold, S.M.; Murthy, P.L.N.; and Bednarcyk, B.A.: Micromechanics-Based Modeling of Laminated SiC/SiC Ceramic Matrix Composites. NASA TM-20210011810, 2021. https://ntrs.nasa.gov
9. Khafagy, K.H.; Sorini, C.; Skinner, T.; and Chattopadhyay, A.: Modeling creep behavior in ceramic matrix composites. Ceramics International, vol. 47, no. 9, 2021, pp. 12651–12660.
10. Santhosh, U.; and Ahmad, J: A model for estimating nonlinear deformation and damage in ceramic matrix composites. Journal of Composite Materials, vol. 47, no. 10, 2012, pp. 1257–1272.
11. Santhosh, U.; Ahmad, J.; Kalarikkal, S.; Ojard, G.; and Gowayed, Y.: Time-Dependent Deformation and Damage Modeling of a SiC/SiC Composite. Journal of Aerospace Engineering, vol. 36, no. 6, 2018, 04018086.
12. Almansour, A.: Use of single tow ceramic matrix minicomposites to determine fundamental room and elevated temperature properties, PhD Dissertation, University of Akron, 2017.
13. Almansour, A.; Maillet, E.; and Morscher, G.N.: Tensile creep and rupture behavior of different fiber content and type single tow SiC/SiC minicomposites. in: D. Singh (Ed.), Mechanical Properties and Performance of Engineering Ceramics and Composites X: A Collection of Papers Presented at the 39th International Conference on Advanced Ceramics and Composites, John Wiley & Sons, Inc., Hoboken, NJ, 2015, pp. 11–19.
14. Lamon, J.; Rebillat, F.; and Evans, A.G.: Microcomposite Test Procedure for Evaluating the Interface Properties of Ceramic Matrix Composites. J. Am. Ceram. Soc., vol. 78, no. 2, 1995, pp. 401–405.
15. Sullivan, R.M.: Time-dependent stress rupture strength of Hi-Nicalon fiber-reinforced silicon carbide composites at intermediate temperatures. J. Eur. Ceram. Soc., vol. 36, 2016, pp. 1885–1892.
16. Kreyszig, Erwin: Advanced Engineering Mathematics. Seventh ed., John Wiley & Sons, New York, NY, 1992.
17. Stouffer, D.C.; and Dame, L.T.; Inelastic Deformation of Metals: Models, Mechanical Properties and Metallurgy, John Wiley & Sons, New York, NY, 1996.